

Observation of extreme field-induced mass deviations in double quantum wells

J. A. Simmons, N. E. Harff,* and J. F. Klem

Sandia National Laboratories, Albuquerque, New Mexico 87185

(Received 11 November 1994; revised manuscript received 10 January 1995)

Large deviations are measured in the cyclotron effective mass m_c near the recently observed partial energy gap arising in strongly coupled GaAs double quantum wells (QW's) subject to in-plane magnetic fields B_{\parallel} . The energy gap results from an anticrossing of the two QW dispersion curves, shifted in \mathbf{k} space relative to one another by B_{\parallel} . The severely distorted dispersion near the gap yields an m_c repressed by more than a factor of 3 near the upper gap edge, and enhanced by $\sim 50\%$ near the lower gap edge. The data show excellent agreement with recent theoretical calculations.

Double-quantum-well (DQW) systems are of interest because they constitute a system in which an additional electronic degree of freedom in the growth direction can be controllably introduced into a two-dimensional electron gas. Most magnetotransport measurements on DQW's have been for high magnetic fields perpendicular to the growth plane B_{\perp} , where the electron's kinetic energies are quenched and Coulomb interactions dominate.¹⁻³ Recent work has investigated the effects of purely in-plane fields B_{\parallel} , in which case single-particle tunneling dynamics dominate the interactions between the two electron layers. The primary effect of B_{\parallel} is a linear transverse shift in the canonical momentum $\hbar\mathbf{k}$ of electrons in one quantum well (QW) relative to the other. This produces a strong modulation⁴⁻⁷ of the tunneling conductance $G_{\perp}(B_{\parallel})$ due to the conservation of energy and in-plane \mathbf{k} .

Very recently, in our previous work⁸⁻¹¹ and in work by Kurobe *et al.*,¹² it was demonstrated that when the interwell coupling is sufficiently strong, a high B_{\parallel} also strongly modulates the in-plane conductance G_{\parallel} . The tunneling causes the shifted dispersion curves of the QW's to anticross, opening a partial energy gap, or minigap, of width ϵ_G . At the edges of the minigap, the electron group velocities are strongly distorted, and the density of states $D(\epsilon)$ forms van Hove singularities. By sweeping B_{\parallel} , the minigap is made to pass through the chemical potential μ , with the singularities in $D(\epsilon)$ producing two sharp features in $R_{\parallel} = G_{\parallel}^{-1}$, a minimum and a maximum as shown in Fig. 1(a), corresponding to the upper and lower gap edges, respectively. The data exhibited excellent agreement with theoretical predictions,⁹ and ϵ_G could be extracted from the data. This system is unusual in that its Fermi surface (FS) has several components, whose shape and number can be tuned by B_{\parallel} . A similarly shaped FS, although not tunable by B_{\parallel} and arising from a different mechanism, was studied many years ago in vicinal planes of Si.¹³

Here we report measurements of the cyclotron mass m_c of electrons near the edges of the field-induced DQW minigap.^{11,14} The masses are measured by adding a small B_{\perp} component to B_{\parallel} , and examining the temperature (T) dependence of the resulting Shubnikov-de Haas (SdH) oscillations. In the upper-energy branch of the dispersion

curve, m_c is greatly repressed, reaching values near the upper gap edge of $< \frac{1}{3}$ of the effective mass of bulk GaAs ($m_{\text{GaAs}}^* = 0.067m_0$, where m_0 is the free-electron mass). In the lower-energy branch m_c is enhanced by $\sim 50\%$ near the lower gap edge, and converges rapidly to m_{GaAs}^* away from the edge. Finally, by measuring the period in $1/B_{\perp}$ of the SdH oscillations, the area of the dominant orbit of the FS is determined as a function of B_{\parallel} . Our data are in excellent agreement with a theoretical calculation by Lyo.¹⁵

The molecular-beam-epitaxy (MBE)-grown sample^{8,10,11} consisted of a modulation-doped pair of GaAs QW's of equal width $w = 150 \text{ \AA}$ separated by an $\text{Al}_{0.3}\text{Ga}_{0.7}\text{As}$ barrier of thickness $t = 25 \text{ \AA}$. Each QW had a density $n \approx 1.5 \times 10^{11} \text{ cm}^{-2}$. The top and bottom QW mobilities were ~ 2.7 and $\sim 2.2 \times 10^5 \text{ cm}^2/\text{V s}$.

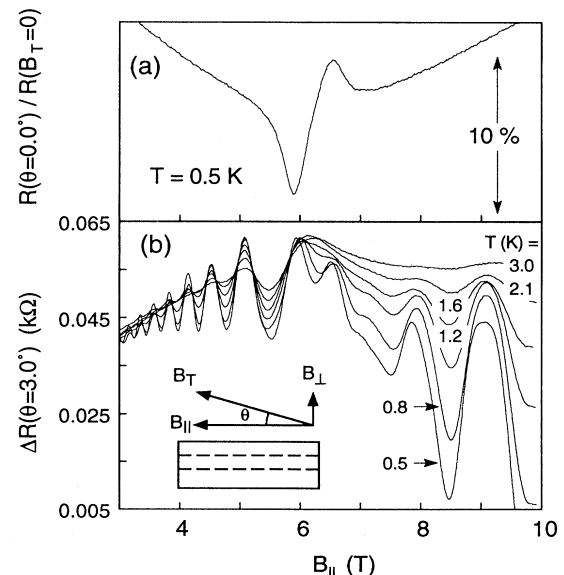


FIG. 1. Normalized R_{\parallel} vs B_{\parallel} for $\theta=0.0^\circ$, showing the anticrossing features. (b) Plot of $\Delta R(B_{\parallel}, \theta=3.0^\circ) = R(B_{\parallel}, \theta=3.0^\circ) - R(B_{\parallel}, \theta=0.0^\circ)$, for several T . At 3.0 K, SdH oscillations occur only for $B_{\parallel} \lesssim 5.9$ T, indicating a dramatically lower mass in this range. The inset shows the experimental geometry.

Four-terminal 17-Hz lock-in measurements were performed in a ^3He cryostat at 12 different T from 0.5 to 3.0 K, as determined with a calibrated Ge thermometer. The excitation current was along the direction of B_{\parallel} . The SdH measurements required a small B_{\perp} , while a large B_{\parallel} was needed to move the minigap through μ . This arrangement was achieved by mounting the sample in a uniform total field B_T at angles $\theta=0.0^\circ, 2.5^\circ, 3.0^\circ$, and 3.5° from parallel, with rotations performed *in situ*.

In Fig. 1(a) we show the normalized in-plane resistance R_{\parallel} , at $T=0.5$ K, as a function of $B_{\parallel}=B_T\cos\theta$, for $\theta=0.0^\circ$. A minimum occurs at $B_{\parallel}=5.9$ T, followed by a maximum at 6.5 T. We now briefly discuss the origin of these two features. Shown in Fig. 2(a) is a tight-binding calculation^{8,9} of the DQW dispersion $\epsilon(k_y)$ at $B_{\parallel}=7.5$ T for our sample parameters, where B_{\parallel} is in the x direction.¹⁶ B_{\parallel} linearly shifts the two QW dispersion curves relative to one another in k_y . The strong inter-QW coupling produces an anticrossing and associated minigap whose width ϵ_G (previously measured to be of order 1 meV) is independent of B_{\parallel} and $=\Delta_{\text{SAS}}$, the zero-field symmetric-antisymmetric gap (SAS).^{8-10,15} The minigap dramatically distorts $D(\epsilon)$ and the electron group velocities [Fig. 2(b)]. Since the upper branch of $\epsilon(\mathbf{k})$ is nearly parabolic, a steplike increase occurs in $D(\epsilon)$ at the upper gap edge. Thus as B_{\parallel} is increased and the gap moves upward, the (low-velocity) states at the upper gap edge eventually pass through μ and are abruptly emptied, greatly reducing the scattering and causing a sharp minimum in R_{\parallel} . By contrast, $\epsilon(\mathbf{k})$ at the lower gap edge is saddle shaped, yielding a logarithmic divergence in $D(\epsilon)$. When B_{\parallel} is further increased and the lower gap edge crosses μ , electrons are divergently scattered into these (zero-velocity) states, yielding the sharp maximum in R_{\parallel} .

The shape of the FS is determined by the intersection of μ and $\epsilon(\mathbf{k})$. For $B_{\parallel} < 5.9$ T, μ lies above the minigap, and the FS has a small lens-shaped orbit lying within a larger hourglass-shaped orbit, shown in Fig. 2(c). For $5.9 \text{ T} < B_{\parallel} < 6.5$ T, μ lies in the gap and only the hourglass orbit is present. As B_{\parallel} is increased further, μ touches the lower gap edge (at the saddle point), causing the hourglass waist to pinch off. For $B_{\parallel} > 6.5$ T, the FS

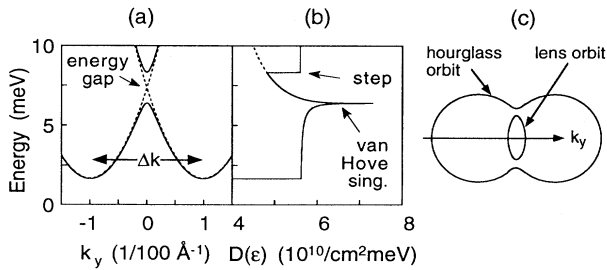


FIG. 2. Calculations for our DQW at $B_{\parallel}=7.5$ T. (a) Dispersion $\epsilon(k_y)$, with (solid lines) and without (dotted lines) coupling. (b) $D(\epsilon)$ for the lower-energy branch (dotted line) and both energy branches (solid line). (c) Sketch of the Fermi surface for $\mu \approx 9$ meV.

separates into two distorted Fermi circles of roughly equal size.

Adding a small B_{\perp} , we probed the cyclotron masses near the minigap edges, where the dispersion is strongly distorted. B_{\parallel} and B_{\perp} could not be swept independently, mixing the SdH oscillations with the anticrossing features. To partially remove this mixing, for each T examined we subtracted the resistance in a purely parallel field [e.g., Fig. 1(a)] from the resistance in a slightly tilted field, to yield $\Delta R(B_{\parallel}, \theta) = R(B_{\parallel}, \theta) - R(B_{\parallel}, \theta=0)$. Figure 1(b) shows $\Delta R(B_{\parallel}, \theta=3.0^\circ)$ for several T . (A small magnetoresistance background remains due to B_{\perp} .) The oscillations are uniform up to ~ 5.9 T; then both the period and amplitude change significantly, indicating a drastic change in m_c when μ crosses the energy gap.

To determine m_c from the T dependence of the SdH oscillations, we first must consider which parts of the FS contribute. While for $B_{\parallel} < 5.9$ T both the lens and hourglass orbits are present, they enclose greatly different areas in \mathbf{k} space. Electrons transverse both these orbits at a rate $d\mathbf{k}/dt = -(e/\hbar)\mathbf{v}_k \times \mathbf{B}_{\perp}$, where \mathbf{v}_k is the Fermi velocity. When θ and hence B_{\perp} are sufficiently small, electrons in the hourglass are unable to traverse the entire orbit without scattering, and so contribute negligibly to the SdH oscillations. Because \mathbf{v}_k is nearly the same for the two orbits (except very close to the gap edge), however, enough electrons complete the lens orbit to produce the SdH oscillations. While the scattering rates for the two orbits may be somewhat different, this assumption agrees with the data for $B_{\parallel} < 5.9$ T, where only a single SdH period is apparent for all three θ . For $5.9 \text{ T} < B_{\parallel} < 6.5$ T, the FS consists of only the hourglass orbit, while for $B_{\parallel} > 6.5$ T the FS consists of two separated Fermi circles of equal size, producing oscillations of the same period and T dependence. Thus for all three field ranges, the SdH oscillations have a single period, and can be analyzed as arising from a single orbit of the FS.

For a single FS orbit, the SdH oscillations are described by¹⁷

$$\frac{\delta R(T)}{4R_0} = \sum_{s=1}^{\infty} \frac{sX_T}{\sinh(sX_T)} \exp\left[\frac{-\pi s}{\omega_c \tau}\right] \cos\left[\frac{2\pi s \mu}{\hbar \omega_c} - \pi s\right], \quad (1)$$

where $\delta R(t)$ is the change in resistance, R_0 is the resistance at $B_{\perp}=0$, $X_T = 2\pi^2 k_B T / \hbar \omega_c$, $\omega_c = eB_{\perp}/m_c$, and τ is the scattering time. When B_{\perp} is sufficiently small that $\omega_c \tau$ is of order unity, the higher-order terms become negligible, and the SdH oscillations become small in amplitude and sinusoidal in shape. This is clearly in accord with our data, where the oscillations are strongly sinusoidal and never exceed 15% of the background.¹⁸

When higher-order terms are negligible, the SdH amplitude is given by¹⁹

$$\frac{\delta R(T)}{\delta R(T_0)} = \frac{T \sinh(\beta T_0 (m_c/m_0)/B_{\perp})}{T_0 \sinh(\beta T (m_c/m_0)/B_{\perp})}, \quad (2)$$

where T_0 is the base temperature and $\beta = 2\pi^2 k_B m_0 / \hbar e$. Figure 3 shows two typical fits of Eq. (2) to $\theta=3.0^\circ$ data.

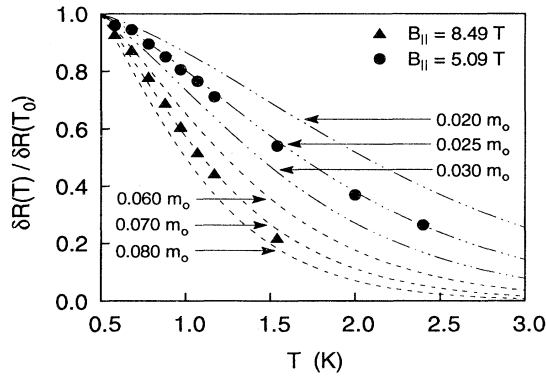


FIG. 3. Measured SdH amplitude δR vs T , at $\theta=3.0^\circ$, normalized to the base $T=0.5$ K. Dashed (dash-dotted) lines show fits of Eq. (2) to $B_{\parallel}=8.49$ T (5.09 T) data for several mass values, with the best fits giving $0.070m_0$ ($0.025m_0$).

[Here δR is determined by taking the difference between $\Delta R(B_{\parallel}, \theta)$ evaluated at adjacent SdH extrema, and subtracting the magnetoresistance background.] While the mass obtained for 8.49 T is $0.070m_0$, that obtained for 5.09 T is $0.025m_0$, a factor of 3 lower than m_{GaAs}^* . The quality of the fits provides further justification for neglecting higher-order terms in Eq. (1). In general, the fits yield masses to roughly $\pm 10\%$ error. For the range $\sim 5.9 \leq B_{\parallel} \leq \sim 6.5$ T, however, the mass changes substantially between adjacent SdH extrema, yielding larger errors of roughly $\pm 20\%$.

Our main experimental result is in Fig. 4, which shows $m_c(B_{\parallel})$ for all three θ . At the lowest B_{\parallel} of 2.7 T, $m_c \approx 0.05m_0$, considerably lower than m_{GaAs}^* . Raising B_{\parallel} causes m_c to decrease, reaching $0.021m_0$ near the upper gap edge at 5.6 T. As B_{\parallel} is increased further, m_c suddenly increases rapidly, reaching a value of $0.099m_0$ just below 6.5 T, where μ crosses the lower gap edge or saddle point. m_c then rapidly converges to m_{GaAs}^* near ~ 7 T, and remains roughly constant thereafter.²⁰

Following Lyo,¹⁵ a qualitative understanding of the behavior of m_c can be gained by examining Fig. 2 and employing the expression $m_c = (\hbar/2\pi) \oint \mathbf{v}_k^{-1} d\mathbf{k}$, where the integration is along the dominant orbit. As B_{\parallel} is increased, the upper gap edge moves upward toward μ . As a result, the size of the inner lens orbit decreases, while \mathbf{v}_k in the denominator decreases more slowly, resulting in a monotonic decrease of m_c . The lens orbit vanishes at 5.9 T when the upper gap edge coincides with μ , but because \mathbf{v}_k also vanishes at this field, m_c does not go to zero. Above 5.9 T, the orbit size increases abruptly as electrons move from the lens to the hourglass, causing an abrupt increase in m_c . As B_{\parallel} increases from 5.9 to 6.5 T, μ lies in the minigap and moves toward the saddle point. At the same time, \mathbf{v}_k becomes smaller near the saddle point, now yielding a monotonic increase of $m_c(B_{\parallel})$. The divergence of m_c at the saddle point, due to \mathbf{v}_k vanishing there, is suppressed in the data by damping. As B_{\parallel} increases beyond 6.5 T, μ falls below the saddle point, causing the hourglass orbit to split into two smaller, roughly

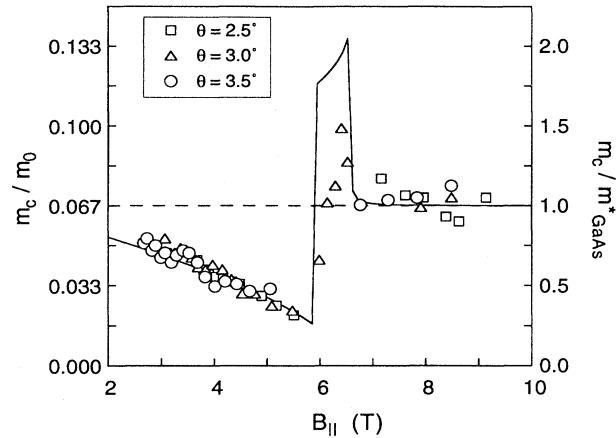


FIG. 4. Summary of measured m_c values vs B_{\parallel} . The solid line is the theoretical calculation of Ref. 15.

circular orbits with nearly parabolic dispersions. The two QW's are thus effectively uncoupled, and m_c approaches m_{GaAs}^* . In Fig. 4 we plot Lyo's calculation of $m_c(B_{\parallel})$ for our sample,¹⁵ where B_{\parallel} has been scaled by 0.96 in order to bring the calculated anticrossing features closer in line with their experimentally observed B_{\parallel} positions. The data are in excellent agreement with the theory.

Finally, we note that the SdH period $\Delta(1/B_{\perp})$ also gives²¹ a measure of the dominant orbit's \mathbf{k} -space area $A = (2\pi e/\hbar) [\Delta(1/B_{\perp})]^{-1}$. In Fig. 5 we plot, as a function of B_{\parallel} , the inverse difference $[\Delta(1/B_{\perp})]^{-1}$ for adjacent SdH extrema which both lie in the same field range. As B_{\parallel} is raised, $[\Delta(1/B_{\perp})]^{-1}$ falls increasingly rapidly as 5.9 T is approached, corresponding to the shrinking lens orbit. In the range $B_{\parallel}=5.9-6.5$ T, too few SdH oscillations are present to determine the orbit area, while for $B_{\parallel} > 6.5$ T, $[\Delta(1/B_{\perp})]^{-1}$ is clearly much larger, and appears constant to within the $\pm 20\%$ error for this range. This is as expected, since here the orbit area is that of ei-

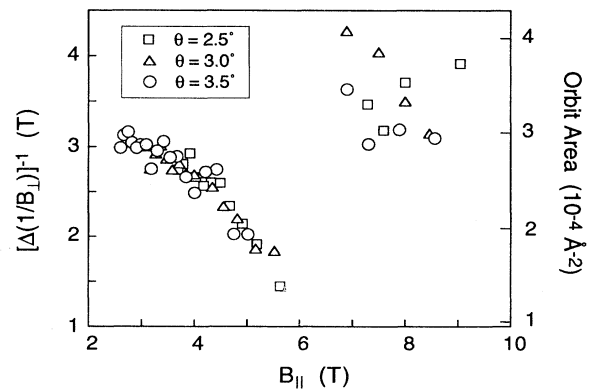


FIG. 5. $[\Delta(1/B_{\perp})]^{-1}$, the inverse spacings in $1/B_{\perp}$ of the SdH minima and maxima, vs B_{\parallel} . The right-hand scale gives the area A of the dominant orbit of the Fermi surface.

ther of the two separated Fermi circles.

In summary, we have measured the cyclotron masses of electrons in a strongly coupled DQW, subject to B_{\parallel} sufficiently high to produce an anticrossing and partial energy gap at μ . Masses near the upper gap edge are suppressed to $< \frac{1}{3}m_{\text{GaAs}}^*$, while masses near the lower gap edge, or saddle point, are enhanced above m_{GaAs}^* by $\sim 50\%$. The data are qualitatively explained by analyzing the changing shape and topology of the B_{\parallel} -dependent

Fermi surface, and show excellent agreement with recent theory.

We thank T. M. Eiles and J. E. Schirber for valuable discussions, T. R. Castillo for excellent technical assistance, and S. K. Lyo for making available his theoretical results prior to publication. This work was supported by the U. S. Dept. of Energy under Contract No. DE-AC04-94AL85000.

*Also at Oregon State University, Corvallis, OR 97331.

¹G. S. Boebinger, H. W. Jiang, L. N. Pfeiffer, and K. W. West, *Phys. Rev. Lett.* **64**, 1793 (1990); Y. W. Suen, J. Jo, M. B. Santos, L. W. Engel, S. W. Hwang, and M. Shayegan, *Phys. Rev. B* **44**, 5947 (1991).

²J. P. Eisenstein, L. N. Pfeiffer, and K. W. West, *Phys. Rev. Lett.* **69**, 3804 (1992).

³S. Q. Murphy, J. P. Eisenstein, G. S. Boebinger, L. N. Pfeiffer, and K. W. West, *Phys. Rev. Lett.* **72**, 728 (1994).

⁴J. Smoliner, W. Demmerle, G. Berthold, E. Gornik, and G. Weimann, *Phys. Rev. Lett.* **63**, 2116 (1989).

⁵J. P. Eisenstein, T. J. Gramila, L. N. Pfeiffer, and K. W. West, *Phys. Rev. B* **44**, 6511 (1991).

⁶J. A. Simmons, S. K. Lyo, J. F. Klem, M. E. Sherwin, and J. R. Wendt, *Phys. Rev. B* **47**, 15741 (1993); S. K. Lyo and J. A. Simmons, *J. Phys. Condens. Matter* **5**, L299 (1993).

⁷K. M. Brown, E. H. Linfield, D. A. Ritchie, G. A. C. Jones, M. P. Grimshaw, and M. Pepper, *Appl. Phys. Lett.* **64**, 1827 (1994).

⁸J. A. Simmons, S. K. Lyo, N. E. Harff, and J. F. Klem, *Phys. Rev. Lett.* **73**, 2256 (1994).

⁹S. K. Lyo, *Phys. Rev. B* **50**, 4965 (1994).

¹⁰S. K. Lyo, J. A. Simmons, and N. E. Harff, in *The Physics of Semiconductors: Proceedings of the 22nd International Conference, Vancouver, 1994*, edited by D. J. Lockwood (World Scientific, Singapore, 1995).

¹¹N. E. Harff, J. A. Simmons, S. K. Lyo, J. E. Schirber, J. F. Klem, and S. M. Goodnick, in *The Physics of Semiconductors: Proceedings of the 22nd International Conference, Vancouver,*

1994 (Ref. 10).

¹²A. Kurobe, I. M. Castleton, E. H. Linfield, M. P. Grimshaw, K. M. Brown, D. A. Ritchie, M. Pepper, and G. A. C. Jones, *Phys. Rev. B* **50**, 4889 (1994).

¹³For a review and references, see T. Ando, A. B. Fowler, and F. Stern, *Rev. Mod. Phys.* **54**, 437 (1982).

¹⁴G. S. Boebinger, A. Passner, L. N. Pfeiffer, and K. W. West, *Phys. Rev. B* **43**, 12673 (1991) studied DQW Fermi-surface distortions using SdH oscillations, but B_{\parallel} was too small to produce an anticrossing energy gap.

¹⁵S. K. Lyo, following paper, *Phys. Rev. B* **51**, 11160 (1995).

¹⁶Including the Hartree term increases the center-to-center distance between the wave functions of the two QW's, thus lowering the B_{\parallel} at which the minigap crosses μ , and reducing ε_G . See Refs. 8 and 9.

¹⁷P. T. Coleridge, R. Stoner, and R. Fletcher, *Phys. Rev. B* **39**, 1120 (1989).

¹⁸A Dingle plot shows a B_{\parallel} -dependent τ , as expected from the changing Fermi surface. (See Ref. 9.) Nevertheless, $\omega_c\tau$ remains of order unity for all fields.

¹⁹T. Ando, A. B. Fowler, and F. Stern, *Rev. Mod. Phys.* **54**, 437 (1982).

²⁰A faint beating in SdH oscillations appears for $B_{\parallel} > 6.5$ T at low T , but is too weak to analyze. We believe this is due to a slight density imbalance, and is responsible for the larger scatter of m_c in this range.

²¹N. W. Ashcroft and N. D. Mermin, *Solid State Physics* (Holt, Rinehart and Winston, New York, 1976), p. 274.